Journal of
Water & Climate Change

IWA PUBLISHING

Journal of Water and Climate Change Vol 14 No 7, 2260 doi: 10.2166/wcc.2023.037

Climate change impact on streamflow and suspended sediment load in the flood-prone river basin

Rajesh Ranjan and Ashok Mishra *

Agricultural and Food Engineering Department, Indian Institute of Technology Kharagpur, Kharagpur, West Bengal, India
*Corresponding author. E-mail: amishra@agfe.iitkgp.ac.in

AM, 0000-0003-4309-7626

ABSTRACT

Understanding the relationship between climate change and changes in streamflow and suspended sediment load (SSL) at the regional scale is critical for future decisions on water resource management. Hence, this study assessed the projected climate change impact on streamflow and SSL based on CMIP6 projections in the flood-prone Mahanadi River Basin (MRB) using the SWAT model. Bias-corrected climate data from five global climate models under medium and extreme shared socioeconomic pathways (SSPs) were utilized as an input to the SWAT model for the baseline (1985–2014), near future (NF, 2020–2046), and mid future (MF, 2047–2073) periods. Rainfall is expected to increase by 2.86% (2.19%) and 13.35% (16.98%) in the NF and MF, respectively, under SSP245 (SSP585). Streamflow and SSL may increase by 6.38% (6.06%) and 4.43% (7.89%) in the NF and by 29.78% (36.90%) and 37% (46.43%) in the MF, respectively, under SSP245 (SSP585) scenario. Also, streamflow and SSL exhibited an increasing trend in most months as well as in most seasons. The findings may be helpful to decision-makers in identifying watershed management plans by offering more information on how climate change affects the hydro-sedimentological processes in a flood-prone river basin.

Key words: CMIP6, ensemble, ET, sediment, streamflow, SWAT

HIGHLIGHTS

- Impact of climate change on streamflow and SSL in a flood-prone river basin is investigated by using CMIP6 projection.
- Increases in rainfall and decline in the diurnal temperature range (DTR) in all the future scenarios are projected.
- Streamflow and SSL are expected to increase in most months under medium and extreme scenarios.
- Streamflow and SSL demonstrated an increasing trend in all the seasons except in summer.

GRAPHICAL ABSTRACT

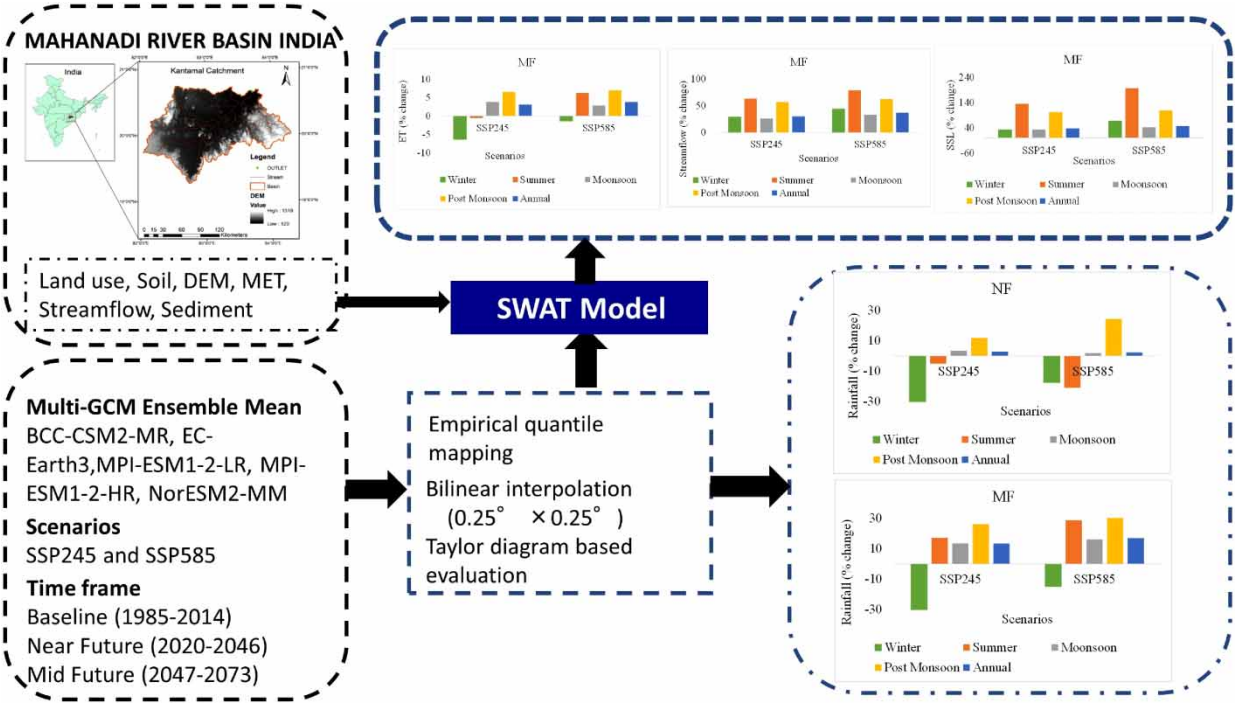

INTRODUCTION

Climate change is a major impediment to achieving sustainable development goals, particularly in nations like India with limited ability to adapt and moderate expertise in managing natural resources. In its sixth Assessment Report (AR6), the Intergovernmental Panel on Climate Change (IPCC) stated that greenhouse gas emissions from human activity have contributed to an average global temperature increase of 1.1 °C or more since 1850–1900. The first two decades of the 21st century (2001–2020) saw an increase in global surface temperature of 0.99 [0.84–1.10] °C, and the last decade (2011–2020) saw an increase of 1.09 [0.95–1.20] °C since 1850–1900. The IPCC also concluded that over the course of the next 20 years, this increase will likely exceed 1.5 °C (IPCC 2021). Climate change is predicted to exacerbate the water cycle, causing changes in streamflow and watershed erosion because of more uneven occurrences of rainfall over time and geography (Nearing *et al.* 2004). Further study on the changes in surface runoff and soil erosion against the backdrop of climate shift is essential to determine the relationship between changing climate and alteration in the streamflow and suspended sediment load (SSL) at a regional scale.

The output of the Global Climate Models (GCMs) based on the Coupled Model Intercomparison Project Phase 5 (CMIP5) has been widely employed to anticipate future climate change and to assess how climate change may affect basin response (Shrestha *et al.* 2016; Jaiswal *et al.* 2017; Bisht *et al.* 2020; Ma *et al.* 2021). However, most CMIP5 GCMs, as well as their ensemble averages, have failed to describe the patterns in Indian summer monsoon rainfall, indicating poor reliability of rainfall estimates (Saha *et al.* 2014; Jain *et al.* 2019). The new climate scenarios based on the combinations of shared socioeconomic pathways (SSPs) and representative concentration pathways (RCPs) have been incorporated into the CMIP6 as part of revisions to the framework for climate modelling research (Van Vuuren *et al.* 2014; Riahi *et al.* 2017). A more improved global carbon cycle, aerosol effects, atmospheric chemistry, terrestrial and marine biogeochemistry, and other processes are included in CMIP6 model, which further enhances each model's physical process and simulation capability (Eyring *et al.* 2016). Also, the performance of the CMIP6 models for the Indian summer monsoon was reported to have improved, with a notable decrease in bias (Gusain *et al.* 2020). There are a few studies that used CMIP6 model projections to investigate climate change impact on the hydro-sedimentology of flood-prone Mahanadi River Basin (MRB) (Pandey *et al.* 2022). Despite improvements in CMIP6, there is still a substantial level of error in climate change scenarios from various GCMs because of inter-model differences, scenario uncertainty, and internal climate variability. Therefore, multi-model

ensembles have been used to capture the wide range of uncertainty leading to increased confidence in the output when examining catchment responses to climate change (Jain *et al.* 2019; Ma *et al.* 2021).

The MRB in India is anticipated to be the most adversely affected Indian River basin by the intensity of floods brought on by changing climate due to its proximity to the Bay of Bengal (Pandey *et al.* 2022). The Hirakud dam and the Mundali weir close to the delta's outlet separate the MRB into three zones: the upper, middle, and delta regions. The upper zone serves as the catchment area of Hirakud dam. The middle Mahanadi Basin is located between the Hirakud dam and the Delta region. Over the previous 10 years, there have been five big floods in the basin (Jena *et al.* 2014). According to the study of historical flood records from 1969 to 2011, streamflow from the middle reaches caused 69% of big floods, the Hirakud dam and middle zone produced 23%, and Hirakud discharges alone caused 8% (Parhi *et al.* 2012). Given the possible negative implications of climate change, a growing body of research has concentrated on how it affects streamflow regimes (including floods) in the MRB (Asokan *et al.* 2016; Jaiswal *et al.* 2017; Bisht *et al.* 2020; Khatun *et al.* 2022; Pandey *et al.* 2022). Nevertheless, much research has not been done on how climate change may affect the amount of sediment produced in the MRB (Dunn *et al.* 2018). Using the global hydrogeomorphic model – WBMsed, Dunn *et al.* (2018) projected the twenty-first century river sediment export to the three deltas in the natural period (without any human interference) from the recent past. Twelve different environmental change scenarios were considered, each of which included a single period for the construction of future reservoirs and combinations of four climates and three socioeconomic paths. The anticipated sediment delivery for the Mahanadi delta increased from 23 to 40 Mt/year (+77%) between the pristine and recent periods, and then it declined from 7 to 25 Mt/year in the last decade of the twenty-first century. Although the WBMsed provides reasonable results globally, it may not always consider local inputs and processes since it is a global model with inputs of very low precision (Dunn *et al.* 2018). Therefore, given the scarcity of climate change assessment investigation and the significance of the catchment, there is a need to evaluate suspended sediment dynamics against the backdrop of climate change at a local scale using catchment level hydro-sedimentological models. Recent years have seen the development of numerous such models, such as the AGNPS (Agricultural Non-Point Source model), SWAT (Soil and Water Assessment Tool), and HSPF (Hydrologic Simulation Program – Fortran) (Young *et al.* 1989; Bicknell *et al.* 1996; Arnold *et al.* 1998). However, the SWAT hydrological program is one of the most tried-and-true, catchment scales, hydrological response unit based, semi-physical, and continuous hydrological programs created to comprehend the implication of climate shift and anthropogenic practices on the watershed process (Tan *et al.* 2020).

Given the foregoing explanation, the present research was carried out to examine the effects of potential climate change under the CMIP6 model projections on the streamflow and SSL from the Kantamal catchment situated within the middle zone of the MRB. This was accomplished by using the SWAT, a widely used hydrological model, in conjunction with climate projections produced by five bias-corrected GCMs for SSP245 and SSP585 climate scenarios for the near future (NF, 2020–2046) and mid future (MF, 2047–2073). The following specific goals were set: (1) To study how the catchment's climate is impacted by climate change, particularly in relation to changes in rainfall and diurnal temperature range (DTR). (2) To investigate how climate change affects ET, streamflow, and SSL on monthly, seasonal, and annual timeframes. Findings of the study may be helpful in enhancing the understanding of the effects of a changing climate on streamflow and SSL in the flood-prone river basin.

MATERIALS AND METHODS

Study area

When it comes to water and sediment export to the Bay of Bengal, Mahanadi is the second-largest river on the Indian Peninsula (Bastia & Equeenuddin 2016). Forty-one monsoonal flood events occurred from 2005 to 2013 in the deltaic region of MRB which highlights the flood vulnerability of this basin (Ghosh *et al.* 2019). There are 14 significant tributaries, of which 12 meet Mahanadi upstream and 2 downstream of the Hirakud dam. The two rivers that converge below the dam are the Tel and the Ong. The Mahanadi River's tributaries had greater streamflow variation, ranging from 0.034 km^3/a in the Hamp to 22.6 km^3/a in the Tel near Kantamal (Bastia & Equeenuddin 2016). This study was conducted in the Kantamal catchment of the MRB, which is in the Odisha state of India (Figure 1). With a 20,235 km^2 area, the catchment is located between latitudes 19°16′10″ to 20°44′42″ N and longitudes 82°02′50″ to 84°30′00″ E. 55% area is occupied by agriculture while forest takes up about 35% of the catchment. The major soil type in the catchment is clay loam (51%). The average annual rainfall is 1,300 mm, the average maximum temperature is 39 °C, and the average minimum temperature is 20 °C. The monsoon season, which lasts from June to September, brings roughly 85 to 90% of the average yearly rainfall.

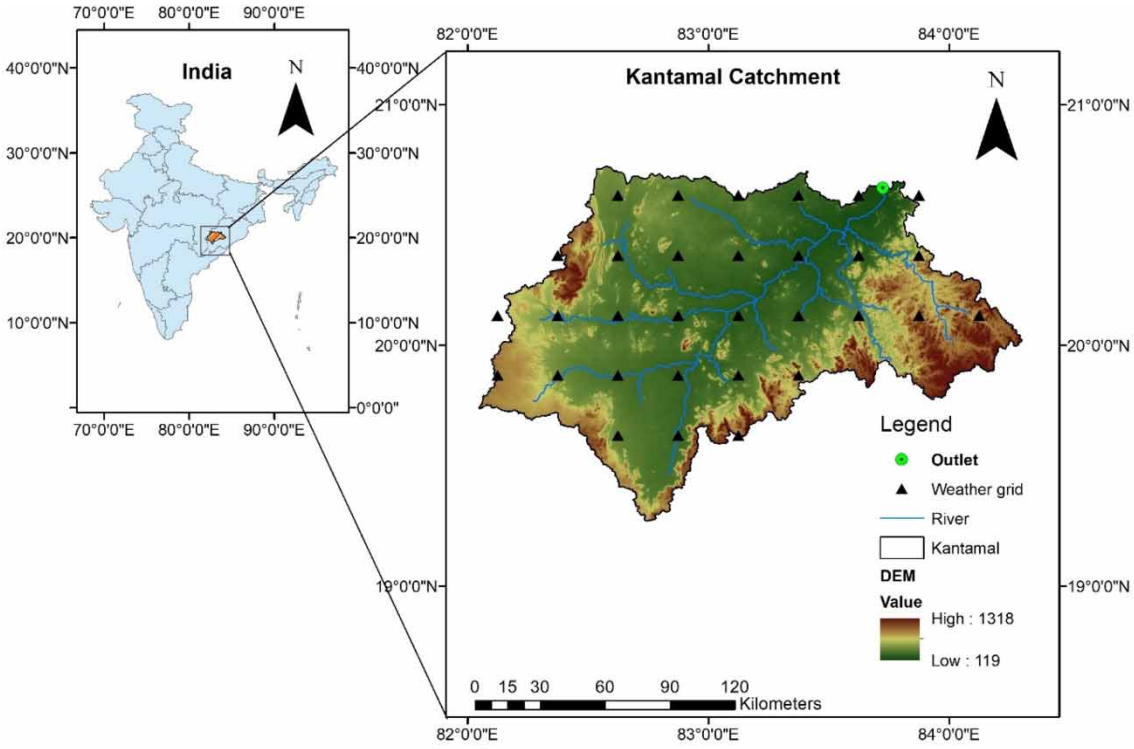

Figure 1 | Study area map with relevant details.

Data used

The SWAT model was set up for the area by using Digital Elevation Model (DEM), land use–land cover (LULC), soil, and weather information. The Shuttle Radar Topography Mission website (http://earthexplorer.usgs.gov) provided the DEM (90 m spatial resolution). The Food and Agriculture Organization (FAO) soil database was used to get soil information at a geographical scale of 1 km by 1 km. LULC of 2005 at a 100 m by 100 m resolution were retrieved from the Distributed Active Archive Center at Oak Ridge National Laboratory (ORNL DAAC) (Das *et al.* 2018). The India Meteorological Department (IMD), Pune, provided the gridded rainfall (0.25° × 0.25°) and temperature (1° × 1°) data used in this investigation (Pai *et al.* 2014). Bilinear interpolation is used to re-grid the 1° × 1° temperature observation to 0.25° × 0.25° to maintain the constant spatial resolution. The daily discharge and sediment data for the period 2000 to 2014, measured at the Kantamal gauging station, were collected from Central Water Commission (CWC), Bhubaneswar.

Climate change data

In order to simulate climate change impact on the hydro-sedimentological fluxes, this study utilized the downscaled bias-corrected climate projections data of five GCMs for historical (1951–2014) and future periods (2015–2073) under two climate scenarios SSP245 and SSP585, representing medium road and high end of range of future pathways, respectively (Mishra *et al.* 2020). All climate datasets were downscaled using bilinear interpolation to the resolution of 0.25° × 0.25° to address the scale mismatch between GCM and IMD datasets. The empirical quantile mapping-based bias-correction method was applied to bilinearly interpolated GCM output to reduce the systematic biases in climate data. The empirical quantile mapping-based bias-correction, non-parametric method has shown better skills than the parametric method in reducing the biases from GCMs (Gudmundsson *et al.* 2012). Mitra (2021) assessed seven CMIP6 models using three measures: (a) Visual Analysis of Prominent Spatial Patterns, (b) Quantitative Analysis of Prominent Spatial Patterns, and (c) Analysis of Spatial Clusters of monsoonal rainfall for the 2000–2014 periods. It was concluded that five models, namely BCC-CSM2-MR, EC-Earth3, MPI-ESM1-2-LR, MPI-ESM1-2-HR, and NorESM2-MM were found to be reasonable for the simulation of rainfall in India. In order to further assess the goodness of fit between bias-corrected GCM data and observed climatic data for the study region, the Taylor diagram was used (Figure 2). The three climate variables (rainfall, T_{max}, and T_{min}) can all be seen to be

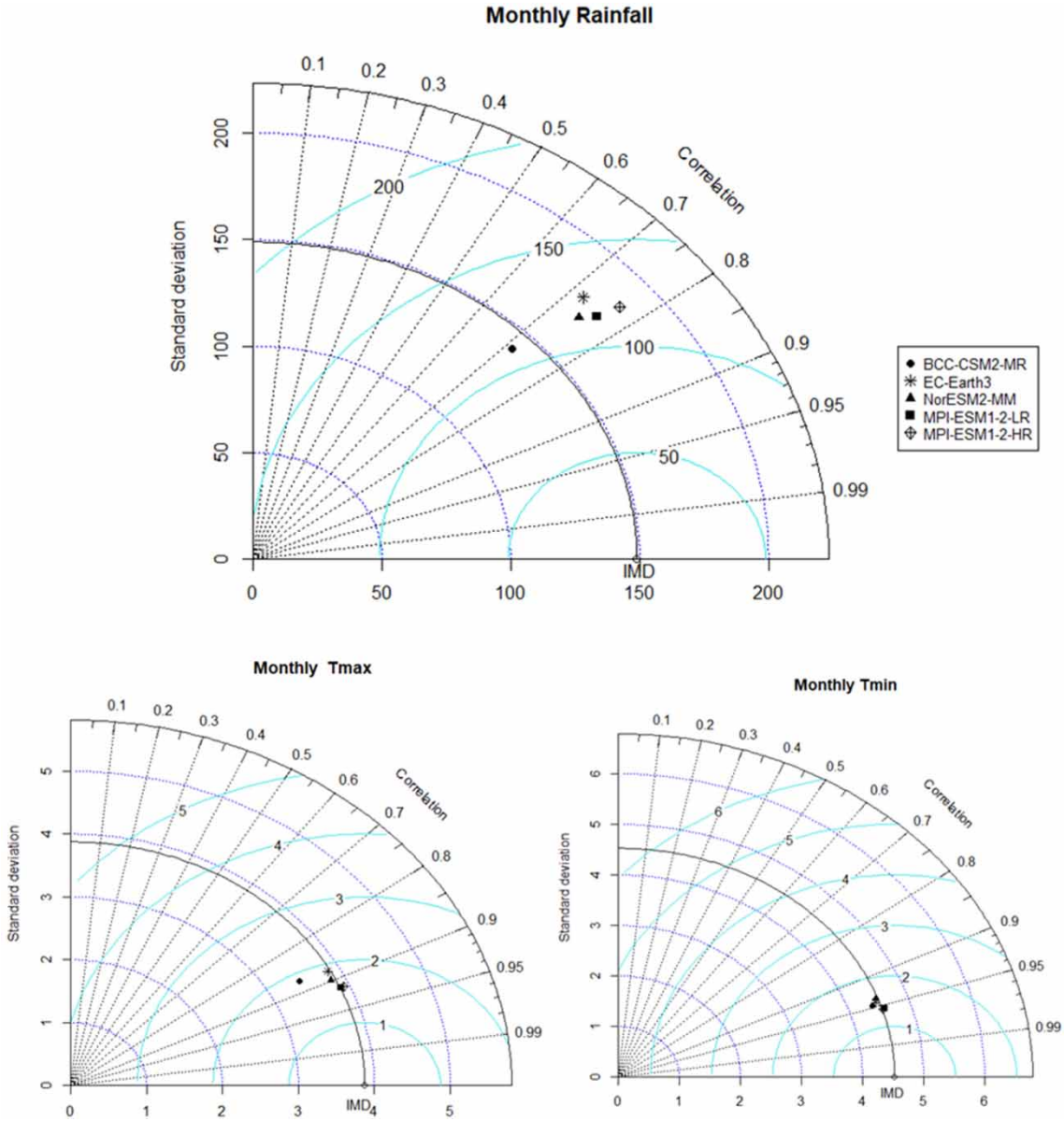

Figure 2 | Evaluation of downscaled and bias-corrected data of five GCMs data using Taylor diagrams.

concentrated closely among the GCMs. The GCMs and the observed variables showed a strong correlation: 0.7–0.8 for rainfall, 0.85–0.95 for T_{max}, and 0.9–0.99 for T_{min}. Hence, these GCMs (listed in Table 1) were selected for climate change impact analysis in this work.

Table 1 | Basic information on CMIP6 GCMs

Sr. No.	GCMs	Country	Institution	Resolution (Lon × Lat)
1	BCC-CSM2-MR	China	Beijing Climate Centre	1.125° × 1.125°
2	EC-Earth3	Europe	EC-Earth-Consortium	0.7° × 0.7°
3	MPI-ESM1-2-LR	Germany	Max Planck Institute for Meteorology	1.9° × 1.9°
4	MPI-ESM1-2-HR	Germany	Max Planck Institute for Meteorology	0.94° × 0.94°
5	NorESM2-MM	Norway	Norwegian Climate Centre	0.94° × 1.25°

SWAT model

The SWAT is a most tried-and-true, catchment scale, hydrological response unit based, semi-physical, and continuous hydrological program created to comprehend the implication of climate shift and anthropogenic practices on watershed processes. SWAT has seen significant revisions since the first edition was released to the public in 1994 (Gassman *et al.* 2007). For detailed information about the SWAT model, one can refer to the theoretical documentation on SWAT (Neitsch *et al.* 2011). To predict surface runoff, evapotranspiration (ET), and streamflow routing in this study, we employed the SCS curve number technique, the Hargreaves & Samani (1985) approach, and variable storage routing methodology, respectively. The Modified Universal Soil Loss Equation (MUSLE) was employed to model soil erosion processes, whereas the Bagnold equation was utilized to characterize channel transport (Neitsch *et al.* 2011). The MUSLE sediment model is as follows:

$$\mathrm{SED_{HRU}} = 11.8 \cdot (Q_{\mathrm{sruf}} \cdot q_{\mathrm{peak}} \cdot \mathrm{area_{hru}})^{0.56} \cdot \mathrm{K} \cdot \mathrm{LS} \cdot \mathrm{C} \cdot \mathrm{P} \cdot \mathrm{CFRG} \quad (1)$$

where $\mathrm{SED_{HRU}}$ is exported sediment from HRU (tons); Q_{sruf} is the runoff volume (mm/ha); q_{peak} is the peak flow ($\mathrm{m^3/s}$); $\mathrm{area_{hru}}$ is the HRU area (ha); terms K, LS, C, P, and CFRG stand for the erodibility factor, slope length factor, land cover factor, support practice factor, and coarse fraction (radius more than 1 mm), respectively, in the universal soil loss equation (USLE).

Model performance evaluation

An incorrect assessment of model performance may be made if only one statistic is used. Visual plots, relative value performance measures, and standardized performance measures are recommended as an alternative way to gauge the goodness of fit (Moriasi *et al.* 2015). Hence, the model performances were evaluated using a variety of goodness-of-fit metrics, including Nash–Sutcliffe Efficiency (NSE), Percentage Bias (PBIAS), Kling-Gupta Efficiency (KGE), coefficient of determination (R^2), and hydrograph comparisons. The other measures were used to assess the model calibration, while the NSE served as a target function. The relationship between the residual variance and the variance of measured data is expressed by this normalized statistic. The NSE value varies between $-\infty$ and 1, with 1 denoting the best possible simulation, 0 implying neutral model performance, and values below zero implying inferior model performance. NSE values of higher than 0.5 for monthly streamflow and sediments were deemed to indicate satisfactory model performance by Moriasi *et al.* (2007). R^2 is a measure of how much spread of the measured data is explained by the model, with 1 being the ideal value. The PBIAS represents the relationship between the mean of the simulated values and the measured values. According to Moriasi *et al.* (2007), 25% for discharge and 55% for sediment reflect good performance ratings while the zero value of PBIAS refers to an ideal condition. Since KGE dissects the NSE score into its separate segments, it may be taken as a refined form of the NSE scores. A more suitable model evaluation is achieved via KGE's multi-component structure, which incorporates linear correlation, bias, and variability into a single target function, in contrast to NSE. The observed mean should be considered as a predictor when KGE < 0.41 (Knoben *et al.* 2019). A performance is regarded as good or intermediate if it scores more than 0.75 or 0.5 on the KGE scale, respectively (Brighenti *et al.* 2019). RMSE-Observations standard ratio (RSR), standardizes RMSE using the standard deviation of observations. RSR value 0 indicates a zero residual variation and therefore perfect model simulation. VE is a fractional volumetric error. Its ideal value is 1.

$$\mathrm{NSE} = 1 - \frac{\sum_{i=1}^{n} (X_{\mathrm{obs},i} - X_{\mathrm{sim},i})^2}{\sum_{i=1}^{n} (X_{\mathrm{obs},i} - \overline{X_{\mathrm{obs}}})^2} \quad (2)$$

$$R^2 = \left[\frac{\sum_{i=1}^{n} (X_{\mathrm{obs},i} - \overline{X_{\mathrm{obs}}})(X_{\mathrm{sim},i} - \overline{X_{\mathrm{sim}}})}{\sqrt[2]{\sum_{i=1}^{n} (X_{\mathrm{obs},i} - \overline{X_{\mathrm{obs}}})^2} \sqrt[2]{\sum_{i=1}^{n} (X_{\mathrm{sim},i} - \overline{X_{\mathrm{sim}}})^2}} \right]^2 \quad (3)$$

$$\mathrm{PBIAS} = \frac{\sum_{i=1}^{n} (X_{\mathrm{obs},i} - X_{\mathrm{sim},i})}{\sum_{i=1}^{n} X_{\mathrm{obs},i}} \times 100 \quad (4)$$

$$\mathrm{KGE} = 1 - \sqrt{(\gamma - 1)^2 + (\alpha - 1)^2 + (\beta - 1)^2} \quad (5)$$

where X is streamflow/SSL, $X_{\mathrm{sim},i}$ is the simulated data at ith month, $X_{\mathrm{obs},i}$ is the observed data at ith month, $\overline{X_{\mathrm{obs}}}$ is the average of observed data, and n is the number of data points under study. α, β, and γ are respectively the ratio of the mean, the ratio of the standard deviation, and correlation coefficient of predicted and observed variables.

Model calibration and validation

Monthly discharge and SSL were used to calibrate the model for the years 2003 to 2011 and to validate it for the years 2012 to 2014. Sensitivity analysis, calibration, and validation were carried out using the SWAT-CUP program. Even though SWAT includes more than 200 parameters, we chose only 22 based on sensitivity analysis result for the SWAT model calibration (Table 2). The 15 most sensitive parameters, in decreasing order, are CH_N2, PRF_BSN, SPCON, CH_K2, ALPHA_BNK, SOL_AWC, SPEXP, ESCO, GW_REVAP, EPCO, CN2, CH_K1, ADJ_PKR, GW_DELAY, and SOL_K. Eight out of 15 sensitive parameters are related to channel processes which implied that the overland flow process is not the dominant driver of streamflow and erosion in this catchment. Fitted parameters are optimized parameters which represent watershed characteristics of MRB. All the fitted parameters are within their physically meaningful range which increases the confidence in the calibrated models. Groundwater delay time (GW_DELAY) for the catchment is defined as the average travel time required for percolated water from the bottom of the soil profile to join the groundwater table through the vadose zone. Its calibrated value is 102.75 days which implied that the water table is at a shallow depth. Groundwater re-evaporation coefficient (GW_REVAP) refers to the rate of movement of water from an unconfined aquifer to the root zone of the soil profile. Its

Table 2 | The calibration parameters and their characteristics

Parameters[a]	Parameter name	Fitted parameter	Original range	
V_GW_DELAY[b]	Groundwater delay time (days)	102.75	2	100
V_ALPHA_BF	Baseflow recession constant (1/days)	0.3345	0.1	0.8
V_GW_REVAP	Groundwater re-evaporation coefficient (–)	0.1482	0.04	0.2
V_RCHRG_DP	Deep aquifer percolation fraction (–)	0.0578	0.2	0.8
R_CN2	Curve number, moisture condition II (–)	0.127	−0.3	0.3
R_SOL_BD	Soil bulk density (g/cm^3)	0.0785	−0.25	0.25
R_SOL_AWC	Soil available water capacity (mm H_2O/mm soil)	0.073	−0.25	0.25
R_SOL_K	Soil hydraulic conductivity (mm/h)	0.0275	−0.35	0.35
R_USLE_K	Soil erodibility (0.013 metric ton m^2 ha/(m^3-metric ton-cm)	−0.0805	−0.25	0.25
V_CH_N2	Manning 'n' for main channels (–)	0.1191	0.03	0.35
V_CH_K2	Effective hydraulic conductivity of the main channel (mm/h)	34.975	10	200
V_ALPHA_BNK	Baseflow alfa factor for bank storage (days)	0.4659	0.2	0.8
V_CH_COV1	Channel erodibility factor (–)	0.322	0.08	0.5
V_CH_COV2	Channel cover factor (–)	0.484	0.005	0.8
V_ESCO	Soil evaporation compensation factor (–)	0.6215	0.2	0.8
V_EPCO	Plant uptake compensation factor (–)	0.6155	0.2	0.8
V_CH_K1	Effective hydraulic conductivity of the tributary channel (mm/h)	91.6038	10	200
V_ADJ_PKR	Peak flow adjustment factor in sub-basin for sediment routing (–)	1.1479	0.6	1.8
V_PRF_BSN	Peak flow adjustment factor in main channel for sediment routing (–)	0.5044	0.2	1.8
V_SPCON	Linear sediment re-entrainment factors for sediment routing (–)	0.0072	0.0005	0.05
V_SPEXP	Exponential sediment re-entrainment factors for sediment routing (–)	1.3196	1.2	1.45
V_USLE_C	USLE cover factor (–)	0.3498	0.02	0.4

[a]*Source*: Neitsch *et al.* (2011).

[b]'R' means original parameter is multiplied by (R + 1) factor, 'V' refers to replacement of the original parameter with the new one.

optimum value was found to be 0.1482 which shows that the groundwater re-evaporation is a significant process in the study area and the saturated zone is not very far below the land surface. Baseflow days are the number of days for baseflow recession to decline through one log cycle. The baseflow recession constant (V_ALPHA_BF) is inversely related to baseflow days and is a direct index of groundwater flow response to changes in recharge. Its optimum value is 0.3345 which indicates slow response. Deep aquifer percolation fraction (V_RCHRG_DP) is fitted to 0.0578 which implies minimal loss of water from catchment to deep aquifer recharge. Curve number (R_CN2) is optimized to 0.127 which results in final CN > 82 for every HRU. This represents a high surface runoff condition present in the study area. Optimized soil parameters also refer to moderately high runoff potential as 97.72% of the study area lies in hydrologic soil group of C. Manning 'n' for main channels (V_CH_N2) is 0.12 which resembles the roughness of natural stream with heavy timber or brushes. The effective hydraulic conductivity of the main channel (V_CH_K2) is 34.975 mm/h, which indicates that the bed and bank material of stream is sand and gravel mixture with low slit-clay content and it supports a moderately high loss rate. The baseflow alpha factor for bank storage (V_ALPHA_BNK) is 0.4659, indicating the moderate recession of bank storage. Bank storage contributes flow to the main channel or reach within the sub-basin. Effective hydraulic conductivity of the tributary channel (V_CH_K1) controls transmission loss from surface runoff as it flows to the main channel in the sub-basin. Its optimized value is 91.6038 mm/h which indicates a high loss rate. The channel erodibility factor (V_CH_COV1) is conceptually similar to the soil erodibility factor in the USLE equation. It is a function of bed/bank material and its optimized value is 0.322 which indicates that the channel provides a moderate high resistance to erosion. Channel cover factor (V_CH_COV2) is defined as the ratio of degradation from a channel with a specified vegetative cover to the corresponding degradation from a channel with no vegetative cover. The vegetation affects degradation by reducing the streamflow velocity and consequently its erosive power near the bed/bank. Its optimised value is 0.484 which indicates that moderate protection is offered by vegetative cover in the stream. Soil evaporation compensation factor (V_ESCO) is calibrated at 0.6215 which indicates a moderate contribution of lower layer soil to meet soil evaporative demand. Plant uptake compensation factor (EPCO) is calibrated at 0.6155 which again shows the moderate contribution of lower layer soil to meet plant water uptake demand. Peak flow adjustment factor in sub-basin for sediment routing (V_ADJ_PKR), peak flow adjustment factor in the main channel for sediment routing (V_PRF_BSN), linear sediment re-entrainment factors for sediment routing (V_SPCON), and exponential sediment re-entrainment factors for sediment routing (V_SPEXP) are calibrated at 1.1479, 0.5044, 0.0072, and 1.3196, respectively, which shows the moderate degradation of the river reach. These parameters are related to sediment routing by the simplified Bagnold equation. The lowest operationally demanding of the SWAT-CUP optimization software is the SUFI-2. It is based on the inverse modelling approach for simultaneous optimization and uncertainty analysis (Wu & Chen 2015) and was used for calibration and validation in this work. The sequential (SQN) calibration method has been employed in most research to simulate SSL and streamflow. However, the Sequential-Simultaneous (SQN_SML) method was tested as superior to the conventional SQN calibration method in terms of improved predictive skills and reduced parameter equifinality (Ranjan & Mishra 2022). Hence, the SQN_SML calibration approach was used in this study.

Methodology for climate change impact assessment

Figure 3 presents the overall framework for examining the impact of climate change on hydro-sedimentological fluxes. By contrasting historical simulations (1985–2014) with future simulations (2020–2073) utilizing anticipated climatological variables from climate models, the effect of climate change on hydro-sedimentological fluxes was evaluated. Climate change impact was investigated for the near future (NF, 2020–2046) and mid future (MF, 2047–2073) under SSP245 and SSP585 scenarios. The hydrological model was run for the historical and future periods with each GCM data and the final output was used in the unweighted ensemble mean for analysis of the climate change impact on hydro-sedimentological fluxes. A warm-up period of 3 years was considered for both historical (1982–1984) and future (2017–2019) period model simulations to reduce the effect of the initial condition. Except for the meteorological data, all other inputs and parameters used during historical and future periods were kept identical to assess the isolated future climate change impact on hydro-sedimentological fluxes.

RESULTS AND DISCUSSION

Model performance

The effectiveness of the model was assessed by comparing the monthly simulated hydrograph and sedimentograph with the corresponding observed data throughout the calibration and validation periods (Figure 4). The simulated values fairly

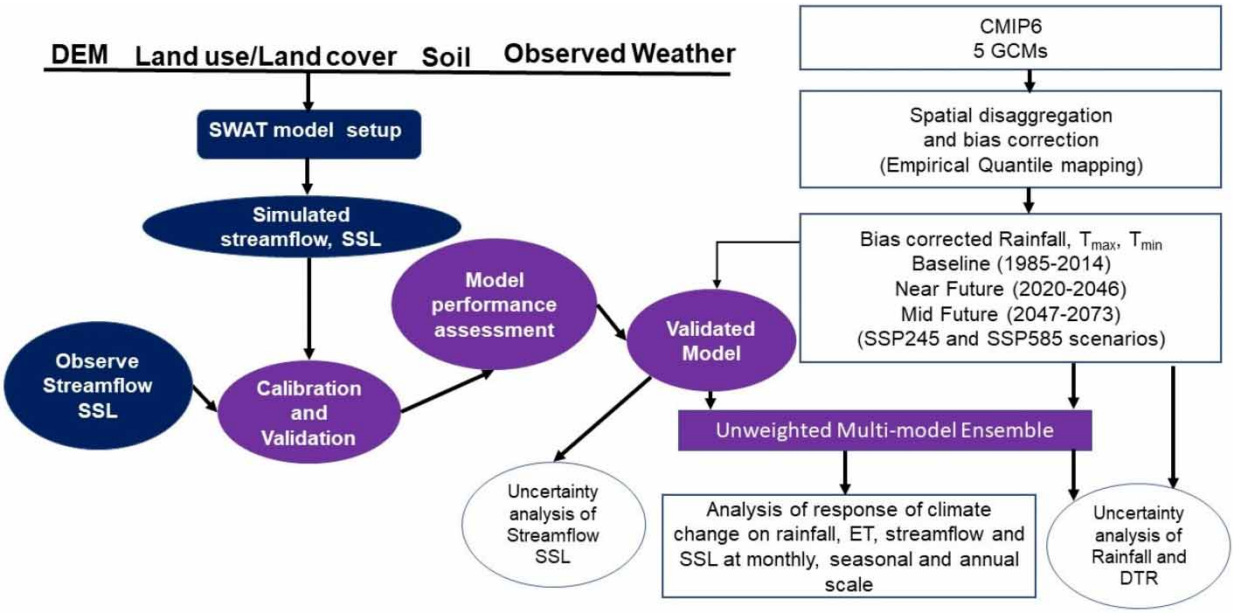

Figure 3 | Framework for climate-hydrological modelling chain.

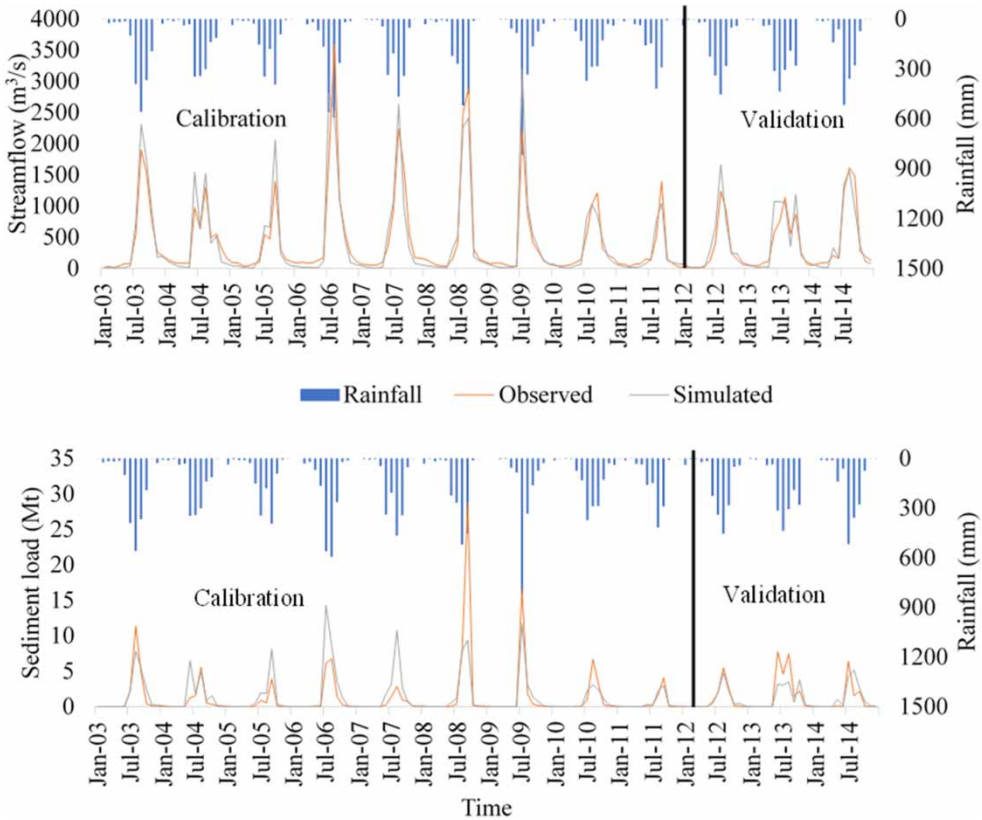

Figure 4 | Comparing simulated streamflow and SSL with observed counterparts during the calibration phase (January 2003–December 2011) and the validation phase (January 2012–December 2014) in the Kantamal catchment using the SQN_SML calibration approach.

Table 3 | Model performance during the calibration and validation phases

Phases	Variable	NSE	PBIAS (%)	RSR	KGE	R^2	VE
Calibration	Streamflow	0.87	0.1	0.36	0.91	0.89	1
	SSL	0.55	−12.5	0.67	0.63	0.55	0.89
Validation	Streamflow	0.85	−6.8	0.39	0.88	0.87	0.94
	SSL	0.65	11.7	0.59	0.64	0.66	1.13

replicated the observed data, except for a few high streamflow/SSL as shown in Figure 4. Table 3 shows the evaluation performance of the model during the calibration and validation periods. The performance of the model for streamflow was found to be excellent with goodness-of-fit statistics: $R^2 = 0.89$, NSE = 0.87, PBIAS = 0.1% RSR = 0.36, KGE = 0.91, and VE = 1 during calibration and $R^2 = 0.87$, NSE = 0.85, PBIAS = −6.8%, RSR = 0.39, KGE = 0.88, and VE = 0.94 during validation. During the calibration period, the simulated SSL agreed with the observed SSL with $R^2 = 0.55$, NSE = 0.55, PBIAS = −12.5%, RSR = 0.67, KGE = 0.63, and VE = 0.89 and with $R^2 = 0.66$, NSE = 0.65, PBIAS = 11.7%, RSR = 0.59, KGE = 0.64, and VE = 1.13 in the validation period. Hence, the simulated monthly SSL demonstrated a satisfactory agreement with the observed SSL (Moriasi *et al.* 2007). Given that sediment modelling is more complex than streamflow modelling, streamflow modelling had better goodness-of-fit ratings than the SSL.

Projected anomaly in rainfall and DTR

Climate change is most visible in rainfall and surface air temperature changes. As a result, the change in annual basin averaged climatic information for two future periods; near future (NF, 2020–2046), and mid future (MF, 2047–2073); with respect to the historical period (1985–2014) was analysed and depicted in Table 4. Expected rainfall was compared to the base period rainfall and the results show that three out of five models projected wetter conditions in the NF for both SSP245 and SSP585 scenarios. Also, all five GCMs, except MPI-ESM1-2-HR, predicted a wetter future in the mid future for both scenarios. This finding agreed with other studies which show the lesser uncertainty in the direction of projected rainfall in MF than NF for MRB (Jin *et al.* 2018; Bisht *et al.* 2020). For NF and MF, respectively, the percentage change in rainfall under SSP245 (SSP585) ranges from −7.75 to 11.08% (−12.97 to 13.73%) and −0.64 to 27.40% (2.8 to 23.49%). The result, using ensemble means of all five models, showed an increased NF rainfall of 2.86% (2.19%) and increased MF rainfall of 13.35% (16.98%) under SSP245 (SSP585) scenarios. Thus, MRB may suffer a wetter climate in both NF and MF provided future climate is unfolded following either of the SSPs. The DTR, defined as the difference between T_{max} and T_{min}, showed a declining trend, irrespective of climatic scenarios and analysis period. The drop in DTR has been identified as an important indicator of how the climate is changing around the world (Braganza *et al.* 2004). The change in DTR varied from −0.44 to −0.01 °C (−0.47 to −0.15 °C) for NF and from −0.53 to −0.12 °C (−0.91 to −0.4 °C) for MF under SSP245 (SSP585). An increase in

Table 4 | Change in rainfall (percentage change) and diurnal temperature range (DTR) of the Kantamal catchment in the middle Mahanadi River Basin under changing climate

	Rainfall (mm)				DTR (°C)			
Variable	SSP245		SSP585		SSP245		SSP585	
Scenarios GCMs/Period	NF	MF	NF	MF	NF	MF	NF	MF
BCC-CSM2-MR	**−7.75**	0.69	**−12.97**	**2.80**	− 0.11	−0.5	−0.29	**−0.91**
EC-Earth3	7.27	16.97	8.21	22.21	**−0.44**	**− 0.53**	**− 0.47**	− 0.82
MPI-ESM1-2-LR	7.51	22.83	6.97	**23.49**	− 0.21	−0.27	−0.37	**−0.4**
MPI-ESM1-2-HR	−3.34	**−0.64**	− 4.36	18.32	−0.15	−0.14	−0.34	**−0.4**
NorESM2-MM	**11.08**	**27.40**	**13.73**	18.87	**−0.01**	**− 0.12**	**− 0.15**	− 0.5
MME	2.86	13.35	2.19	16.98	−0.19	−0.31	−0.32	−0.6
Uncertainty	18.83	28.04	26.7	26.29	0.43	0.41	0.32	0.51

Bold values represent minimum and maximum projected change under a scenario.

projected minimum temperatures was more than the increase in projected maximum temperatures, resulting in a decline in the DTR in all future scenarios. This finding is in line with the previous studies which indicated that climate change was closely associated with a greater increase in the minimum temperature than the maximum temperature, and thus a widespread decline in DTR was observed in almost all parts of the globe during the past decades (Sun *et al.* 2021; Liu *et al.* 2022). Also, DTR in the MRB was reported to be declining by Bisht *et al.* (2020).

Implication of climate change on annual streamflow and SSL

Climate change impact analysis of the annual hydro-sedimentological fluxes in the Kantamal catchment under the SSP245 and SSP585 scenarios with five GCMs revealed mixed signals for both streamflow and SSL; however, the directions of change for streamflow and SSL were the same (Table 5). Also, change in rainfall is accompanied by proportional change in streamflow both in terms of magnitude and direction.

NorESM2-MM projected the highest increase in streamflow (69.72%) and sediment load (106.44%) in MF under the SSP245 scenario as a result of the highest projected rainfall (Table 4). For NF and MF, respectively, the percentage change in streamflow under SSP245 (SSP585) ranges from −13.70 to 26.28% (−22.63 to 35.18%) and −5.47 to 69.72% (5.09 to 54.44%). Similarly, the percentage change in SSL under SSP245 (SSP585) ranges from −19.31 to 27.17% (−26.92 to 56.16%) and −17.19 to 106.44% (5.85 to 65.59%) for NF and MF, respectively. Uncertainty in the rainfall projection (range of projected rainfall) is found to be lower than that of streamflow and uncertainty in projected SSL is greater than that of streamflow under both SSPs and timeframes. Propagation of uncertainty down the cascading modelling chain may be attributed to the enlargement of error in SSL. Under SSP245 (SSP585), the mean ensemble result showed an increase in streamflow by 6.38% (6.06%) in the NF and an increase by 29.78% (36.90%) for the MF, as well as an increase in SSL by 4.43% (7.89%) for the NF and an increase by 37% (46.43%) for the MF. Our results corroborated with Pandey *et al.* (2022) which reported much higher streamflow under CMIP6 climate projection in the MRB that may result in frequent future floods.

Implication of climate change on monthly ET, streamflow, and SSL

Figure 5 shows the anticipated average monthly ET, streamflow, and SSL under SSP245 and SSP585 for the near and mid futures, as well as their anomaly from the historical period. Mean monthly ET was projected to decrease in the NF under both SSPs from January to July except April. The decrease in ET despite the increase in temperature may be attributed to drought situation caused by the decrease in the rainfall during the first half of calendar year. The percentage decrease in ET ranges from −0.1% (−1.21%) in July to −8.34% in January (−7.26% in June) under SSP245 (SSP585) in NF (Figure 5(a)). The percentage increase in ET in the NF ranges from 0.42 to 6.77% (0.53 to 4.18%) under SSP245 (SSP585) with the highest increase expected in October. The increase in ET during August to December in the NF may be caused by flooding situation in these months. Thus, MRB may experience drought in the first half and flood in the latter half of the calendar year in NF under both SSPs. The decrease in ET is projected in the first 4 months in SSP245 and in the first 2 months in SSP585 in the

Table 5 | Change in annual streamflow and SSL (percentage change) of the Kantamal catchment in the middle Mahanadi River Basin under changing climate

Variable	Streamflow				SSL			
Scenarios	SSP245		SSP585		SSP245		SSP585	
GCMs/Period	NF	MF	NF	MF	NF	MF	NF	MF
BCC-CSM2-MR	**−13.70**	−0.25	**−22.63**	**5.09**	**− 19.31**	− 3.00	**−26.92**	**5.85**
EC-Earth3	11.09	29.58	14.10	43.96	12.42	35.48	14.33	53.80
MPI-ESM1-2-LR	19.93	57.78	17.47	**54.44**	**27.17**	70.01	22.69	**65.59**
MPI-ESM1-2-HR	−10.50	**−5.47**	− 12.73	37.66	−18.07	**−17.19**	− 22.71	49.71
NorESM2-MM	**26.28**	**69.72**	**35.18**	43.50	23.95	**106.44**	**56.16**	57.65
MME	6.38	29.78	6.06	36.90	4.43	37.00	7.89	46.43
Uncertainty	39.98	75.19	57.81	59.53	46.48	123.63	83.08	71.44

Bold values represent minimum and maximum projected change under a scenario.

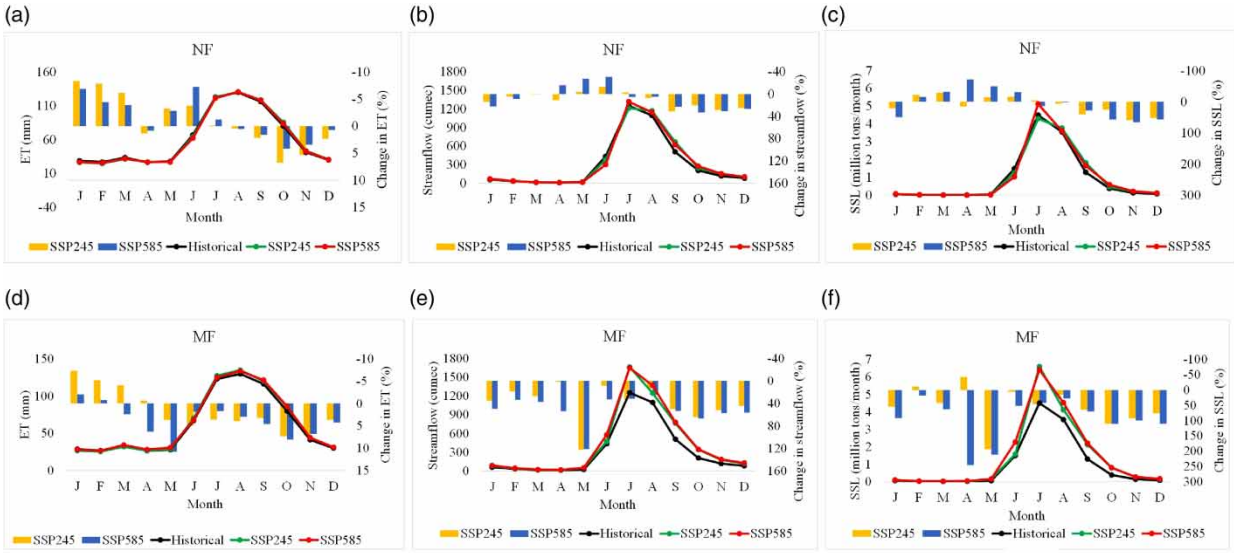

Figure 5 | Average monthly ET (a, d), streamflow (b, e), and SSL (c, f) for historical (1985–2014), near future (NF, 2020–2046), and mid future (MF, 2047–2073) and their respective percentage change in future concerning the historic period.

MF. The decrease in monthly ET varied from −0.63% in April to −7.4% in January (−0.78% in February to −2.05% in January) while the increase in ET varied from 3.22% in September to 7.34% in October (1.66% in July to 10.77% in May) under SSP245 (SSP585) in MF (Figure 5(d)). The increase in ET may be attributed to increased rainfall in the majority of months in the MF. All months except March, May, June, and July (March, April, May, and June) are expected to have an increasing trend of streamflow in the NF under SSP245 (SSP585) (Figure 5(b)). Monthly streamflow is expected to increase (from 1.15% in April to 122% in May under SSP245 and from 25% in August to 121% in May under SSP585) in all the months in MF (Figure 5(e)). The increase in streamflow under both SSPs is more visible in the months of September to November in the NF and in the months of July to November in MF. These results are in-line with the findings by Jin *et al.* (2018), who reported that the impact of climate may be more in the months of September to November in the 2050s. Ghosh *et al.* (2010) also projected that floods frequency may increase in most climate scenarios in MF in the MRB. Also, peak streamflow and SSL occurred in the same month of July under both historical as well as future time periods. The highest increase in sediment load is expected in May as a result of the highest increase in the streamflow in May in MF under both SSPs (Figure 5(f)). The projected change in streamflow and SSL is comparatively higher in the MF than in the NF. Thus, the impact of climate change on streamflow and SSL is projected to be more prominent in the MF than in the NF. The trend of change of SSL is the same as that of streamflow in the flood season, however the range of variation in SSL is much higher than that of streamflow because of the non-linear relation between streamflow and SSL.

Implication of climate change on seasonal rainfall, ET, streamflow, and SSL

The impact of climate change on seasonal rainfall, ET, streamflow, and SSL was performed on the seasonal scale employing four sub-sample time series of JJAS, OND, JF, and MAM months. These months have distinct rainfall characteristics and represent monsoon, post-monsoon, winter, and summer seasons, respectively. Due to high rainfall during southwest monsoon (90% of annual rainfall happens in this season), seasonally projecting the change in hydro-sedimentology of the catchment from the perspective of future climate change is essential. Also, the seasonal streamflow and sediment yield reveal the impact of future climate change more clearly than the monthly due to the larger time horizon (Sinha *et al.* 2020; Sreedevi *et al.* 2022). Figure 6 shows predicted seasonal and annual anomaly in future rainfall, ET, streamflow, and SSL using the ensemble mean of all GCMs. Rainfall (ET) is projected to decrease in winter and summer by −31.13% (−8.1%) and −5.13% (−3%) under SSP245 and by −17.56% (−5.7%) and −21% (−2.12%) under SSP585 in NF (Figure 6(a) and 6(b)). The highest increase in rainfall (ET) by 11.8% (5.5%) under SSP245 and by 24.29% (3.29%) under SSP585 is expected in the post-monsoon season in NF. The highest increase in rainfall (ET) by 26.13% (6.54%) under SSP245 and by 34.82%

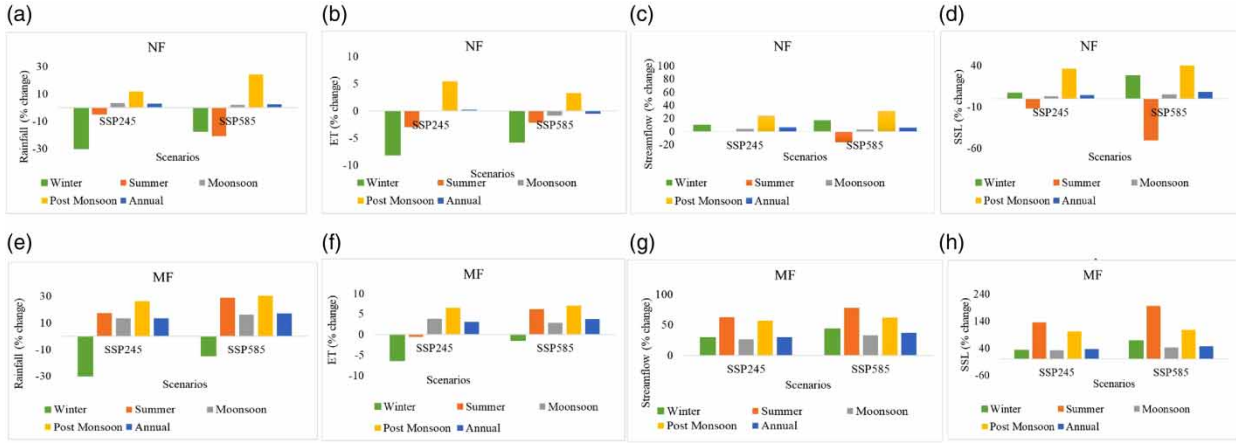

Figure 6 | Changes in rainfall (a, e), ET (b, f), streamflow (c, g), and sediment load (d, h) as a percentage of historic levels utilising ensemble averages for SSP245 and SSP585 scenarios for the four seasons of winter (JF), summer (MAM), monsoon (JJAS), and post-monsoon (OND) and at annual time scale in the Kantamal catchment.

(6.98%) under SSP585 is expected in the post-monsoon season in MF (Figure 6(e) and 6(f)). The direction of change of streamflow and SSL are the same at seasonal and annual scales under both SSPs and time frames. However, this may not be essential. The previous study revealed that the direction of change of streamflow and sediment under climate change may not be the same (Shrestha *et al.* 2016; Sreedevi *et al.* 2022) because the sediment generation and transport are not only the function of rainfall and streamflow but also plant growth and sediment connectivity. A decrease in rainfall but an increase in temperature causes a drought situation, leading to weathering due to drying of soil and decay of plants thereby creating a favourable condition for the soil erosion. In contrast, an increase in rainfall and temperature leads to vigorous plant growth and thereby decreases the erosion. A change in rainfall and temperature causes a change in the sediment transport capacity of river and erosion rate which in turn leads to a change in sediment load carried by the river. Under wetter and warmer conditions, where more transport capacity is coupled with a greater erosion rate, higher sediment flux is anticipated (Zhu *et al.* 2008). Streamflow is projected to change by 10.36% (17.32%) in the winter, by 0.73% (−16.02%) in summer, by 4.23% (3%) in the monsoon, and by 23.62% (31%) in the post-monsoon season (Figure 6(c)) and SSL are projected to change by 6.67% (27.56%) in the winter, by −11.78% (−50.62%) in summer, by 2.8% (5.4%) in the monsoon, and by 36.24% (58.79%) in the post-monsoon season (Figure 6(d)) under SSP245 (SSP585) scenarios in the NF period. For the MF period, streamflow are projected to increase by 29.21% (43.85%) in the winter, by 62.94% (78.33%) in summer, by 25.97% (32.96%) in the monsoon, and by 56.61% (62%) in the post-monsoon season (Figure 6g) while SSL is projected to increase by 32.7% (67.11%) in the winter, by 135% (196.63%) in summer, by 32.93% (42.03%) in the monsoon, and by 101.74% (108.2%) in the post-monsoon season (Figure 6h) under SSP245 (SSP585) scenarios. Despite rainfall reduction in a few seasons, streamflow and SSL showed an expected increase in most seasons in the MF as well as in the NF period as a decline in the rainfall is accompanied by the reduction in the ET in those few seasons. Streamflow and SSL showed an increasing trend under all seasons in MF with the highest increase in the summer under both SSPs (Figure 6g and 6h). An increase in SSL in the winter season may be attributed to channel erosion while an increase in SSL in monsoon and post-monsoon may be due to hillslope as well as channel erosion. Rainfall, streamflow, and SSL showed a comparatively higher increase in the MF than in the NF in the monsoon and post-monsoon season and at the annual scale which is also reported by Bisht *et al.* (2020). Frequency of flood events may become greater in the post-monsoon season as compared to monsoon seasons. Among all seasons, the percentage change in rainfall, ET, streamflow, and SSL is projected to be least in the monsoon season. This may be due to the large absolute value of these variables in the largest season, i.e. monsoon season. Therefore, a small percentage change may cause a large deviation in absolute value. Rainfall is the dominant driver of streamflow generation in the post-monsoon season, as despite the increase in ET, streamflow is increasing under all scenarios. This is also true for MF under both SSPs. ET is the dominant driver of streamflow generation in the winter season, as despite the decrease in rainfall, streamflow is increasing under all scenarios.

SUMMARY AND CONCLUSIONS

Given that the MRB is among the most climate-vulnerable regions, it is crucial to comprehend how climate change may affect the MRB's hydro-sedimentological processes. Hence, this study analysed the response of streamflow and SSL to changing climate by using the sequential-simultaneous method followed by the calibrated SWAT model. Bias-corrected historical and future climatic data from five GCMs under SSP245 and SSP585 pathways were utilized in the SWAT model for the baseline (1985–2014), near future (NF, 2020–2046), and mid future (MF, 2047–2071) periods. Mean ensemble GCMs scenarios utilised research findings showing that MRB will experience a warmer and wetter climate in future with less uncertainty in MF than in NF. Consequently, streamflow and SSL are also projected to increase with a higher anomaly in the MF than in the NF under both SSPs. Uncertainty in projected SSL (46.48%–123.63%) is found to be greater than the error in streamflow (39.98–75.19%) which is greater than the uncertainty in projected rainfall (18.83–28.04%). Under all seasons except the summer, streamflow and SSL demonstrated an upward trend. This suggests that the flood problem in the Kantamal catchment may worsen in the future, given the increase in streamflow under most scenarios which has also been reported by Pandey *et al.* (2022). Furthermore, the increasing trend of SSL may reduce the storage capacity of the river body, resulting in frequent flooding of the Kantamal catchment and increasing the likelihood of delta stability against the sea level rise. A more pronounced increase of rainfall in the post-monsoon in comparison to the monsoon season may aggravate the flooding situation in the downstream deltaic region as the catchment is already saturated with monsoonal rainfall, so opportunities for abstraction loss are much less in the post-monsoon season. This may cause an increased frequency of flooding in the post-monsoon season in the near future as compared to monsoonal floods. Historically, only 6 of 41 monsoonal flood events have occurred in the first half of October from 2005 to 2013 (Ghosh *et al.* 2019). Precipitation and ET, respectively, were found to be the dominant drivers of streamflow generation in post-monsoon and winter seasons under the changing climate. The major takeaways of this study are as follows:

(1) Although the study area does not have any major reservoirs, release from the Hirakud reservoir which lies upstream of the study area may worsen the flooding situation in the already vulnerable delta region. Therefore, this study provides important input to reservoir operation planning of Hirakud dam under the potential future climate change condition. Monthly and seasonal projections of evapotranspiration, streamflow, and SSL under most recent CMIP6-SSP scenarios may be helpful in adapting the rule curve of the reservoir in view of the changing climate. As the highest increase in rainfall, streamflow, and SSL are expected in the post-monsoon season, instead of the monsoon season, the rule curve may be tweaked to provide additional flood control reservoir storage for mitigating the flood hazard.
(2) Seasonality of rainfall and ET are projected to be more amplified, i.e. wet season may get wetter while dry season may get drier. This may lead to flood-drought alteration events in the MRB, especially in the near future. As the study area is predominantly agricultural (55% of basin area) with the major crop rice grown throughout the year, this study is helpful in adapted irrigation/agricultural planning in view of the projected flood-drought situation.
(3) The projected change in SSL reveals the severity of the erosion issues in the catchment. Waterbodies may become more silted as a result of these changes. Geomorphological changes in rivers and floodplains may also have an adverse effect on riparian ecosystems and communities. Intricate sediment management techniques such as best management practices may become more necessary as a result of the possible increase in erosion, which could potentially impede agricultural expansion. These anticipated scenarios offer substantial guidance for natural resource planning and management, enhancing the environmental, social, and economic well-being of the catchment.

Concerning streamflow and SSL in the flood-prone river basin, this work offers a valuable assessment of the consequences of a changing climate under the latest CMIP6 model projections. By advancing knowledge of adaptability in the context of a changing climate, the findings may also help put into practice and plan streamflow and sediment management measures. Additionally, the study is limited by the uncertainties associated with the emission scenario, GCMs, bias-correction technique, and hydrological modelling. Uncertainty due to the choice of hydrological model may be mitigated through the multi-model approach (Georgakakos *et al.* 2004). This also facilitates the identification of a better model for large-scale catchment sediment simulation. The copula-based zero inflated rainfall bias-correction method may be employed to mitigate the error due to the choice of bias correction as this technique is found to be better in preserving both the mean and extreme rainfall characteristics for a geography characterized by tropical monsoon-type rainfall pattern with a large proportion of daily rainfall time-series data of zero values (Maity *et al.* 2019; Suman & Maity 2021). Therefore, one of the critical goals of our future study should be to investigate uncertainty and improve confidence in the accuracy of the climate change

impact outcome of flood-prone basin. The effect of future LULC change is not considered in our study. Several previous studies have demonstrated that climate change has greater impacts on catchment behaviour than land use change in the large river basin (Wagner *et al.* 2013; Ma *et al.* 2021; Sreedevi *et al.* 2022). However, changes in land use do affect the hydro-sedimentological process of the basin. Therefore, it is essential to gain an understanding of independent effects of LULC and climate change on hydro-sedimentological fluxes as well as their combined effects to lessen soil erosion during monsoon season and maintain water availability during the rest of the year.

ACKNOWLEDGEMENTS

The authors would like to acknowledge the Central Water Commission (CWC), Bhubaneswar and India Meteorological Department (IMD) for providing the necessary data to carry out this research. The data used in this study can be accessed by these agencies after fulfilling their data-sharing policy. The climate projection data have been collected from https://zenodo.org/record/3987736#.Y34U0nZBxPY. The fellowship to the first author provided by the Ministry of Human Resources Department (MHRD), Government of India is highly acknowledged.

DATA AVAILABILITY STATEMENT

All relevant data are included in the paper or its Supplementary Information.

CONFLICT OF INTEREST

The authors declare there is no conflict.

REFERENCES

Arnold, J. G., Srinivasan, R., Muttiah, R. S. & Williams, J. R. 1998 Large area hydrologic modeling and assessment part I: model development 1. *JAWRA Journal of the American Water Resources Association* **34**, (1) 73–89.

Asokan, S. M., Rogberg, P., Bring, A., Jarsjö, J. & Destouni, G. 2016 Climate model performance and change projection for freshwater fluxes: comparison for irrigated areas in Central and South Asia. *Journal of Hydrology: Regional Studies* **5**, 48–65.

Bastia, F. & Equeenuddin, S. M. 2016 Spatio-temporal variation of water flow and sediment discharge in the Mahanadi River, India. *Global and Planetary Change* **144**, 51–66.

Bicknell, B. R., Imhoff, J. C., Kittle, J., Donigian, A. S. & Johansen, R. C. 1996 *Hydrological Simulation Program – FORTRAN, User's Manual for Release 11*. US Environmental Protection Agency. Environmental Research Laboratory, Athens, Georgia.

Bisht, D. S., Mohite, A. R., Jena, P. P., Khatun, A., Chatterjee, C., Raghuwanshi, N. S., Singh, R. & Sahoo, B. 2020 Impact of climate change on streamflow regime of a large Indian river basin using a novel monthly hybrid bias correction technique and a conceptual modeling framework. *Journal of Hydrology* **590**, 125448.

Braganza, K., Karoly, D. J. & Arblaster, J. M. 2004 Diurnal temperature range as an index of global climate change during the twentieth century. *Geophysical Research Letters* **31** (13), 217.

Brighenti, T. M., Bonumá, N. B., Grison, F., de Almeida Mota, A., Kobiyama, M. & Chaffe, P. L. B. 2019 Two calibration methods for modeling streamflow and suspended sediment with the swat model. *Ecological Engineering* **127**, 103–113.

Das, P., Behera, M. D., Patidar, N., Sahoo, B., Tripathi, P., Behera, P. R., Srivastava, S. K., Roy, P. S., Thakur, P., Agrawal, S. P. & Krishnamurthy, Y. V. N. 2018 Impact of LULC change on the runoff, base flow and evapotranspiration dynamics in eastern Indian river basins during 1985–2005 using variable infiltration capacity approach. *Journal of Earth System Science* **127** (2), 1–19.

Dunn, F. E., Nicholls, R. J., Darby, S. E., Cohen, S., Zarfl, C. & Fekete, B. M. 2018 Projections of historical and 21st century fluvial sediment delivery to the Ganges-Brahmaputra-Meghna, Mahanadi, and Volta deltas. *Science of the Total Environment* **642**, 105–116.

Eyring, V., Bony, S., Meehl, G. A., Senior, C. A., Stevens, B., Stouffer, R. J. & Taylor, K. E. 2016 Overview of the Coupled Model Intercomparison Project Phase 6 (CMIP6) experimental design and organization. *Geoscientific Model Development* **9** (5), 1937–1958.

Gassman, P. W., Reyes, M. R., Green, C. H. & Arnold, J. G. 2007 The soil and water assessment tool: historical development, applications, and future research directions. *Transactions of the ASABE* **50** (4), 1211–1250.

Georgakakos, K. P., Seo, D. J., Gupta, H., Schaake, J. & Butts, M. B. 2004 Towards the characterization of streamflow simulation uncertainty through multimodel ensembles. *Journal of Hydrology* **298** (1–4), 222–241.

Ghosh, S., Raje, D. & Mujumdar, P. P. 2010 Mahanadi streamflow: climate change impact assessment and adaptive strategies. *Current Science* **98** (8), 1084–1091.

Ghosh, A., Das, S., Ghosh, T. & Hazra, S. 2019 Risk of extreme events in delta environment: a case study of the Mahanadi delta. *Science of the Total Environment* **664**, 713–723.

Gudmundsson, L., Bremnes, J. B., Haugen, J. E. & Engen-Skaugen, T. 2012 Downscaling RCM precipitation to the station scale using statistical transformations – a comparison of methods. *Hydrology and Earth System Sciences* **16** (9), 3383–3390.

Gusain, A., Ghosh, S. & Karmakar, S. 2020 Added value of CMIP6 over CMIP5 models in simulating Indian summer monsoon rainfall. *Atmospheric Research* **232**, 104680.

Hargreaves, G. H. & Samani, Z. A. 1985 Reference crop evapotranspiration from temperature. *Applied Engineering in Agriculture* **1** (2), 96–99.

IPCC. 2021 Summary for policymakers. In: *Climate Change 2021: The Physical Science Basis. Contribution of Working Group I to the Sixth Assessment Report of the Intergovernmental Panel on Climate Change* (Masson-Delmotte, V., Zhai, P., Pirani, A., Connors, S. L., Péan, C., Berger, S., Caud, N., Chen, Y., Goldfarb, L., Gomis, M. I., Huang, M., Leitzell, K., Lonnoy, E., Matthews, J. B. R., Maycock, T. K., Waterfield, T., Yelekçi, O., Yu, R. & Zhou, B., eds.). Cambridge University Press, Cambridge, UK and New York, NY, USA, pp. 3–32.

Jain, S., Salunke, P., Mishra, S. K. & Sahany, S. 2019 Performance of CMIP5 models in the simulation of Indian summer monsoon. *Theoretical and Applied Climatology* **137** (1), 1429–1447.

Jaiswal, R. K., Tiwari, H. L. & Lohani, A. K. 2017 Assessment of climate change impact on rainfall for studying water availability in upper Mahanadi catchment, India. *Journal of Water and Climate Change* **8** (4), 755–770.

Jena, P. P., Chatterjee, C., Pradhan, G. & Mishra, A. 2014 Are recent frequent high floods in Mahanadi basin in eastern India due to increase in extreme rainfalls? *Journal of Hydrology* **517**, 847–862.

Jin, L., Whitehead, P. G., Rodda, H., Macadam, I. & Sarkar, S. 2018 Simulating climate change and socio-economic change impacts on flows and water quality in the Mahanadi River system, India. *Science of the Total Environment* **637**, 907–917.

Khatun, A., Ganguli, P., Bisht, D. S., Chatterjee, C. & Sahoo, B. 2022 Understanding the impacts of predecessor rain events on flood hazard in a changing climate. *Hydrological Processes* **36** (2), e14500.

Knoben, W. J., Freer, J. E. & Woods, R. A. 2019 Inherent benchmark or not? Comparing Nash–Sutcliffe and Kling–Gupta efficiency scores. *Hydrology and Earth System Sciences* **23** (10), 4323–4331.

Liu, L., Dong, Z., Gong, H., Wang, L., Chen, W. & Wu, R. 2022 Climatology and trends of wintertime diurnal temperature range over East Asia in CMIP6 models: evaluation and attribution. *Atmospheric Research* **280**, 106438.

Ma, D., Qian, B., Gu, H., Sun, Z. & Xu, Y. P. 2021 Assessing climate change impacts on streamflow and sediment load in the upstream of the Mekong River basin. *International Journal of Climatology* **41** (5), 3391–3410.

Maity, R., Suman, M., Laux, P. & Kunstmann, H. 2019 Bias correction of zero-inflated RCM precipitation fields: a copula-based scheme for both mean and extreme conditions. *Journal of Hydrometeorology* **20** (4), 595–611.

Mishra, V., Bhatia, U. & Tiwari, A. D. 2020 Bias-corrected climate projections for South Asia from Coupled Model Intercomparison Project-6. *Scientific Data* **7** (1), 1–13.

Mitra, A. 2021 A comparative study on the skill of CMIP6 models to preserve daily spatial patterns of monsoon rainfall over India. *Frontiers in Climate* **3**, 654763.

Moriasi, D. N., Arnold, J. G., Van Liew, M. W., Bingner, R. L., Harmel, R. D. & Veith, T. L. 2007 Model evaluation guidelines for systematic quantification of accuracy in watershed simulations. *Transactions of the ASABE* **50** (3), 885–900.

Moriasi, D. N., Gitau, M. W., Pai, N. & Daggupati, P. 2015 Hydrologic and water quality models: performance measures and evaluation criteria. *Transactions of the ASABE* **58** (6), 1763–1785.

Nearing, M. A., Pruski, F. F. & O'neal, M. R. 2004 Expected climate change impacts on soil erosion rates: a review. *Journal of Soil and Water Conservation* **59** (1), 43–50.

Neitsch, S. L., Arnold, J. G., Kiniry, J. R. & Williams, J. R. 2011 *Soil and Water Assessment Tool Theoretical Documentation Version 2009*. Texas Water Resources Institute, College Station, TX.

Pai, D. S., Sridhar, L., Rajeevan, M., Sreejith, O. P., Satbhai, N. S. & Mukopadhyay, B. 2014 Development of a new high spatial resolution long period daily gridded rainfall data set over Indian and comparison with existing data over the region. *Mausam* **65**, 1–18.

Pandey, D., Tiwari, A. D. & Mishra, V. 2022 On the occurrence of the observed worst flood in Mahanadi River basin under the warming climate. *Weather and Climate Extremes* **38**, 100520.

Parhi, P. K., Mishra, S. K., Singh, R. & Tripathy, V. K. 2012 Floods in Mahanadi river basin, Orissa (India): a critical review. In *India Water Week, Water, Energy and Food Security: Call for Solutions*, 10–14 April 2012, New Delhi.

Ranjan, R. & Mishra, A. 2022 Examining model performances and parameter uncertainty for streamflow and suspended sediment regime simulation: comparison of three calibration methods. *Journal of Hydrology* **612**, 128304.

Riahi, K., Van Vuuren, D. P., Kriegler, E., Edmonds, J., O'neill, B. C., Fujimori, S., Bauer, N., Calvin, K., Dellink, R., Fricko, O., Lutz, W., Popp, A., Cuaresma, J. C., KC, S., Leimbach, M., Jiang, L., Kram, T., Rao, S., Emmerling, J., Ebi, K., Hasegawa, T., Havlik, P., Humpenöder, F., DaSilva, L. A., Smith, S., Stehfest, E., Bosetti, V., Eom, J., Gernaat, D., Masui, T., Rogelj, J., Strefler, J., Drouet, L., Krey, V., Luderer, G., Harmsen, M., Takahashi, K., Baumstark, L., Doelman, J. C., Kainuma, M., Klimont, Z., Marangoni, G., Lotze-Campen, H., Obersteiner, M., Tabeau, A. & Tavoni, M. 2017 The shared socioeconomic pathways and their energy, land use, and greenhouse gas emissions implications: an overview. *Global Environmental Change* **42**, 153–168.

Saha, A., Ghosh, S., Sahana, A. S. & Rao, E. P. 2014 Failure of CMIP5 climate models in simulating post-1950 decreasing trend of Indian monsoon. *Geophysical Research Letters* **41** (20), 7323–7330.

Shrestha, B., Cochrane, T. A., Caruso, B. S., Arias, M. E. & Piman, T. 2016 Uncertainty in flow and sediment projections due to future climate scenarios for the 3S Rivers in the Mekong Basin. *Journal of Hydrology* **540**, 1088–1104.

Sinha, R. K., Eldho, T. I. & Subimal, G. 2020 Assessing the impacts of historical and future land use and climate change on the streamflow and sediment yield of a tropical mountainous river basin in South India. *Environmental Monitoring and Assessment* **192**, 1–21.

Sreedevi, S., Eldho, T. I. & Jayasankar, T. 2022 Physically-based distributed modelling of the hydrology and soil erosion under changes in landuse and climate of a humid tropical river basin. *CATENA* **217**, 106427.

Suman, M. & Maity, R. 2021 Assessment of basin-wise future agricultural drought status across India under changing climate. *Journal of Water and Climate Change* **12** (6), 2400–2421.

Sun, X., Wang, C. & Ren, G. 2021 Changes in the diurnal temperature range over East Asia from 1901 to 2018 and its relationship with precipitation. *Climatic Change* **166** (3), 1–17.

Tan, M. L., Gassman, P. W., Yang, X. & Haywood, J. 2020 A review of SWAT applications, performance and future needs for simulation of hydro-climatic extremes. *Advances in Water Resources* **143**, 103662.

Van Vuuren, D. P., Kriegler , E., O'Neill, B. C., Ebi, K. L., Riahi, K., Carter, T. R., Edmonds, J., Hallegatte, S., Kram, T., Mathur, R. & Winkler, H. 2014 A new scenario framework for climate change research: scenario matrix architecture. *Climatic Change* **122** (3), 373–386.

Wagner, P. D., Kumar, S. & Schneider, K. 2013 An assessment of land use change impacts on the water resources of the Mula and Mutha Rivers catchment upstream of Pune, India. *Hydrol. Earth Syst. Sci.* **17**, 2233–2246.

Wu, H. & Chen, B. 2015 Evaluating uncertainty estimates in distributed hydrological modeling for the Wenjing River watershed in China by GLUE, SUFI-2, and ParaSol methods. *Ecological Engineering* **76**, 110–121.

Young, R. A., Onstad, C. A., Bosch, D. D. & Anderson, W. P. 1989 AGNPS: a nonpoint-source pollution model for evaluating agricultural watersheds. *Journal of Soil and Water Conservation* **44** (2), 168–173.

Zhu, Y. M., Lu, X. X. & Zhou, Y. 2008 Sediment flux sensitivity to climate change: a case study in the Longchuanjiang catchment of the upper Yangtze River, China. *Global and Planetary Change* **60** (3–4), 429–442.

First received 20 December 2022; accepted in revised form 6 June 2023. Available online 19 June 2023